# Forecasts of Valley Circulations Using the Terrain-Following and Step-Mountain Vertical Coordinates in the Meso-Eta Model

JEROME D. FAST

*Pacific Northwest National Laboratory, Richland, Washington*

(Manuscript received 15 October 2002, in final form 15 April 2003)

ABSTRACT

The nonhydrostatic version of the NCEP Meso-Eta Model is used to perform simulations that differ by only the vertical coordinate to determine the differences in forecasted valley circulations associated with the step-mountain and terrain-following vertical coordinates and whether one coordinate produces consistently superior forecasts at meso-$\gamma$ and micro-$\alpha$ scales. A horizontal grid spacing of 850 m is used. The model forecasts are evaluated using data from the October 2000 Vertical Transport and Mixing (VTMX) field campaign in the Salt Lake valley. The forecasts of the diurnal evolution of the dominant circulations in the Salt Lake valley, including valley, slope, and canyon flows, and their modification by synoptic forcing during five intensive observation periods, were qualitatively similar to the measurements. Forecasts produced by the step-mountain and terrain-following vertical coordinates each have their own advantages and disadvantages and neither vertical coordinate outperformed the other overall. In general, the terrain-following coordinate simulations reproduced the observed surface wind directions over the valley sidewalls better, while the step-mountain coordinate simulations of nighttime near-surface temperatures and wind speeds were closer to the observations. Significant differences in wind speed and direction between the simulations were also produced in the middle valley atmosphere at night, with the terrain-following coordinate simulations somewhat better than the step-mountain coordinate simulations. Similar forecast errors produced by both simulations probably resulted from the physical parameterizations, rather than the choice of vertical coordinate.

## 1. Introduction

The most widely used mesoscale models, such as the fifth-generation Pennsylvania State University–National Center for Atmospheric Research (Penn State–NCAR) Mesoscale Model (MM5; Dudhia 1993), the Advanced Regional Prediction System (ARPS; Xue et al. 2000), and the Regional Atmospheric Modeling System (RAMS; Pielke et al. 1992), handle topography by various forms of the traditional ''terrain following'' vertical coordinate. In these coordinate systems, the horizontal pressure gradient comprises two terms, of which both are large over steep slopes. It has been known for decades that an inconsistent discretization of these terms can fail to properly account for the partial compensation between them, producing large errors in the horizontal momentum equations (Pielke 1984). A number of alternative approaches for calculating the pressure gradient force in the sigma coordinate have been proposed to minimize these errors (e.g., Carroll et al. 1987; Danard et al. 1993; Mahrer 1984), but success has been limited and these alternative approaches are rarely incorporated into mesoscale models. The numerical treatment of the pressure gradient term and other horizontal gradients may be one factor contributing to forecast errors made by mesoscale models in areas of complex terrain where the slopes are often relatively steep.

Another approach is the ''step mountain'' coordinate, also known as the ''eta'' coordinate, which was adopted by the National Centers for Environmental Prediction (NCEP) as the basis for its operational Eta Model (Black 1994; Janjić 1994; Mesinger et al. 1988; Rogers et al. 1996). Eta Model forecasts have been evaluated previously for a wide range of atmospheric phenomena including synoptic and mesoscale precipitation (e.g., Mesinger 1996; Mesinger and Black 1992), surface winds over the Great Lakes (O'Conner et al. 1999), sea breezes over Florida (Manobianco and Nutter 1999), and boundary layer properties over Illinois (Angevine and Mitchell 2001). Mesinger and Black (1992) found that the precipitation forecasts that employed the step-mountain coordinate were better than the ones produced using the terrain-following coordinate.

Gallus and Klemp (2000), however, found that the step-mountain coordinate did not properly simulate mountain-induced gravity waves when compared to analytic theory and simulations that employed the terrain-following coordinate. The flow did not properly descend along the lee slope because of artificial vorticity pro-

*Corresponding author address:* Dr. Jerome D. Fast, Pacific Northwest National Laboratory, P.O. Box 999, K9-30, Richland, WA 99352. E-mail: jerome.fast@pnl.gov

duced at the corner of each step. Similarly, Gallus (2000) showed that the step-mountain coordinate produced weaker mountain waves and lower wind speeds than the terrain-following coordinate and observations when simulating a downslope windstorm along the Front Range of the Rocky Mountains. While the 10-km version of the Eta Model produced strong subsidence associated with a windstorm along the Wasatch Front in Utah, momentum was not transferred downward to produce strong winds at the ground (Staudenmaier and Mittelstadt 1997). The debate over the choice of vertical coordinate and model performance has led NCEP to use a hybrid sigma–pressure coordinate (Janjić et al. 2001) for operational forecasts nested within the larger domain of the Eta Model and to develop alternative approaches for future operational models (Michalakes et al. 2001).

Most evaluations of the step-mountain coordinate have been for synoptic and mesoscale processes using a horizontal grid spacing greater than 10 km. There has been little documentation, however, on the advantage of the step-mountain coordinate for small-scale simulations. Because of the continuing increase in computational power, operational models like the Eta Model will likely be run at successively finer resolutions in the near future. Therefore, there is a need for in-depth studies of the performance of the step-mountain coordinate in simulating boundary layer properties and circulations affected by basins and valleys, which are common topographic features in the western United States. Evaluating high-resolution simulations is problematic because of the sparse operational measurements of wind, temperature, and humidity in areas of complex terrain. Extensive observations collected during field campaigns, however, are available that can be used to evaluate the performance of operational models in simulating valley circulations.

In this study, simulations that differ only by the vertical coordinate are performed to determine the differences in valley circulations associated with the step-mountain and terrain-following vertical coordinates and to determine whether one coordinate produces consistently superior forecasts at meso-$\gamma$ and micro-$\alpha$ scales. The nonhydrostatic NCEP Meso-Eta Model is used for this purpose because its code has been set up to easily switch between the step-mountain and terrain-following coordinates, so that the differences in the model results can be attributed solely to the use of different coordinate systems. The model forecasts are evaluated using data from the October 2000 Vertical Transport and Mixing (VTMX) field campaign in the Salt Lake valley. To the author's knowledge, this study is also the first evaluation of the Meso-Eta Model's performance with grid spacing smaller than 1 km. The objective of the paper is to describe the forecasts for each vertical coordinate. In contrast with previous evaluations of the Eta Model that usually focused on precipitation forecasts, the present study examines thermally driven circulations in complex terrain and the effect of synoptic forcing on those circulations during clear-sky conditions. Cloud processes, therefore, do not complicate the evolution of the observed and predicted boundary layer.

## 2. VTMX field campaign

As described by Doran et al. (2002), a meteorological field campaign sponsored by the U.S. Department of Energy's (DOE) Atmospheric Sciences Program was recently conducted in the Salt Lake valley to improve the understanding of the nocturnal boundary layer and the boundary layer during morning and evening transition periods. A wide range of remote sensing and in situ measurements were made including those from surface meteorological stations, sonic anemometers, temperature dataloggers, rawinsondes, tethered balloons, radar wind profilers, sodars, and lidars. Much of the instrumentation operated continuously during October 2000. Instruments that required hands-on attention or generated large amounts of data were operated only during intensive operational periods (IOPs). Ten IOPs were conducted during the month; most began in the late afternoon at 2200 UTC [1500 mountain standard time (MST)] and ended the following morning at 1600 UTC (0900 MST).

Diurnal thermally driven circulations, including nocturnal downslope, downvalley, and canyon flows, were observed when the synoptic forcing was weak. Data from this field campaign provide useful information on the dynamics and thermodynamics in an urban valley that cannot be obtained from current operational measurement networks.

## 3. Numerical experiments

The nonhydrostatic version of the NCEP Eta Model, known as the Meso-Eta Model, is used in this study. In contrast with other research mesoscale models, Meso-Eta is primarily an operational model and therefore has a fixed set of turbulence, cloud, land surface, and radiation parameterizations. The domain chosen for this study encompassed the Salt Lake valley, where most of the VTMX field campaign measurements were made, and the surrounding mountain ranges with a grid spacing of about 850 m. The NCEP 32-km Eta analyses provided the initial conditions and 3-h boundary conditions.

The model topography is shown in Fig. 1, along with the actual topography obtained from the U.S. Geological Survey. Salt Lake City is surrounded by the Wasatch Mountains to the east, the Oquirrh Mountains to the west, the Traverse Range to the south, and the Great Salt Lake to the north. The model captures the main topographic variations in the region, but the narrow canyons east of Salt Lake City (Parleys, Big Cottonwood, and Little Cottonwood) are not fully resolved with the current grid spacing.

An example of the vertical grid spacing over the center of the valley below 5 km MSL is shown in Fig. 2

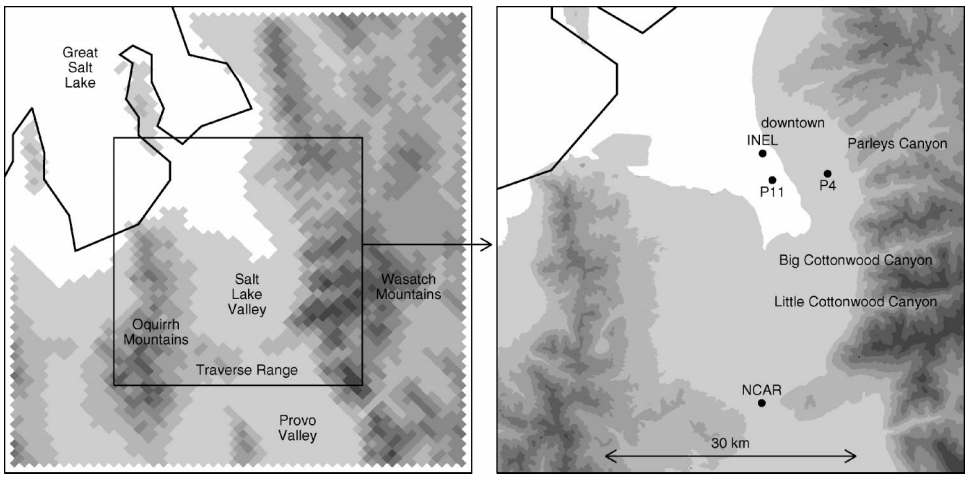


FIG. 1. (left) Domain employed by the Meso-Eta Model and topography from the 45-level step-mountain coordinate and (right) actual topography in the vicinity of Salt Lake City. Here, P4, P11, INEL, and NCAR denote meteorological instrumentation sites employed in this study.

and listed in Table 1. Simulations were primarily performed using 45 vertical layers for both the step-mountain and terrain-following coordinates. These two sets of simulations are referred to as S45 (step mountain) and T45 (terrain following). By default, the model sets the bottom of the step-mountain coordinate's lowest layer at sea level. Since Salt Lake City is located about 1300 m MSL, many of the grid points would be located below ground level and the vertical grid spacing in the lower valley atmosphere would be rather coarse. Therefore, the step-mountain vertical coordinate was modified (M. Pyle 2002, personal communication) so that the first layer was just below the lowest elevation shown in Fig. 1. In this way, the number of vertical layers within the valley atmosphere for both vertical coordinates was the same.

The Meso-Eta Model was run in the S45 and T45 configurations for IOPs 5, 6, 7, 8, and 10 (14–15, 16–17, 17–18, 19–20, and 25–26 October 2000). Each simulation started at 1200 UTC, 10 h before the start of the IOP, and was run for a 36-h forecast period. An additional simulation was made for IOPs 6 and 7, which occurred on consecutive nights. In this case, the model was initialized at 1200 UTC and run for a 60-h period to produce a continuous boundary layer evolution over a multiday period that included both IOPs.

Simulations were also performed for the 60-h period of IOPs 6 and 7 and the 36-h period of IOP 10 using 60 layers for the step-mountain coordinate (Fig. 2) and they are referred to as S60. Simulation S60 had about twice as many grid points in the valley atmosphere as simulation S45, but the number of layers above 2 km AGL for each simulation was the same. By comparing the S45 and S60 simulations, the effect of vertical resolution in the Salt Lake valley can be determined. Ideally, it would be useful to also perform a 60-layer terrain-following coordinate simulation, but this is not an option available in the workstation version of the model.

## 4. Results

For brevity, a comparison of the model forecasts with a select set of observations is presented next to highlight the main differences between the step-mountain and terrain-following coordinate simulations. The evaluation focuses on the performance of the Meso-Eta Model in predicting thermally driven circulations within the Salt Lake valley and their modification by synoptic forcing.

### *a. IOPs 6 and 7: Terrain-induced circulations*

Well-developed diurnal valley, slope, and canyon flows were observed by the measurement network during IOPs 6 and 7 as a result of the light synoptic winds that prevailed over most of the 2-day period. A comparison of the surface winds and temperatures from the 60-h simulation with surface observations from up to 60 sites over a portion of the model domain for an afternoon and a nighttime period is shown in Figs. 3 and 4. Winds and temperatures were measured at 32 sites, while the other 28 sites measured only temperature.

During the afternoon (Fig. 3) at 2300 UTC (1600 MST), the surface winds observed over the valley floor were from the north and northwest, representing lake breezes (Doran et al. 2002) superimposed on the upvalley flow. Upslope and upcanyon flows developed at the stations near the base of canyons along the western slope of the Wasatch Mountains. The near-surface afternoon winds and temperatures predicted by simulations S45 and T45 were quite similar. However, the location of the maximum wind speeds indicate that the upvalley

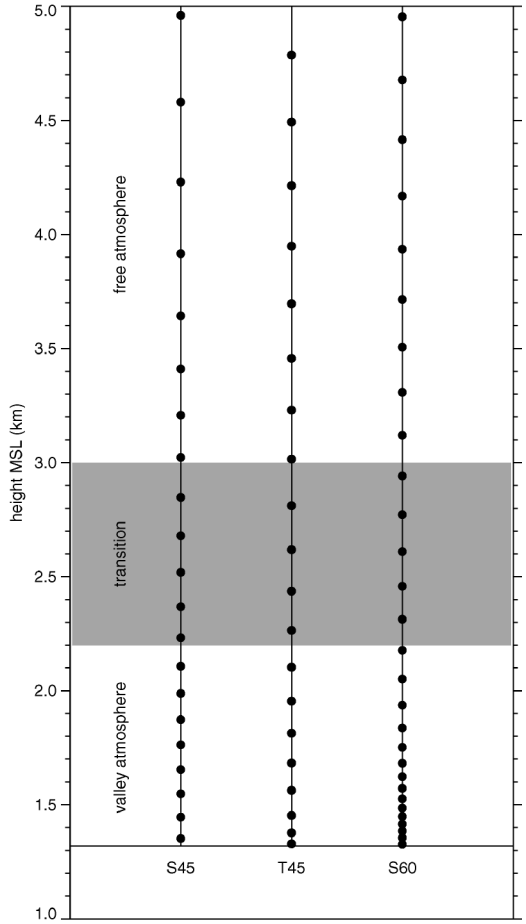


FIG. 2. Location of vertical grid points below 5 km MSL in simulations S45, T45, and S60 over the center of the valley. Gray shading denotes the range of elevations of the surrounding mountain peaks.

TABLE 1. Location of the vertical grid points in simulations S45, T45, and S60 over the center of the valley corresponding to Fig. 2.

| | Height AGL (m) | | |
|---|---|---|---|
| Level | S45 | T45 | S60 |
| 1 | 32 | 9 | 7 |
| 2 | 126 | 57 | 35 |
| 3 | 228 | 133 | 65 |
| 4 | 334 | 243 | 96 |
| 5 | 443 | 363 | 129 |
| 6 | 553 | 493 | 165 |
| 7 | 668 | 634 | 206 |
| 8 | 787 | 783 | 252 |
| 9 | 912 | 944 | 303 |
| 10 | 1048 | 1116 | 362 |
| 11 | 1198 | 1298 | 432 |
| 12 | 1359 | 1491 | 516 |
| 13 | 1527 | 1695 | 616 |
| 14 | 1703 | 1910 | 731 |
| 15 | 1887 | 2137 | 857 |
| 16 | 2090 | 2376 | 993 |
| 17 | 2323 | 2629 | 1138 |
| 18 | 2596 | 2894 | 1290 |
| 19 | 2910 | 3173 | 1451 |
| 30 | 3260 | 3466 | 1621 |

flow from the terrain-following coordinate simulation propagated southward earlier than in the step-mountain coordinate simulation. At the southern end of the valley the observed winds and predicted winds from the step-mountain coordinate shifted from southerly to northerly at 2200 UTC (1500 MST), but the wind shift occurred 1 h earlier in the terrain-following coordinate simulation (not shown). While both the observed and simulated surface temperatures varied by as much as 4°C over the valley floor, the predicted maximum temperatures were 1°–4°C lower than observed.

The observed winds reversed direction at night (Fig. 4) with southeasterly winds over the valley floor, southwesterly downslope flows over the gentle slopes of the western valley, and easterly downslope and canyon flows over the steeper slopes at the base of the Wasatch Mountains at 0900 UTC (0200 MST). Winds over the valley center were generally much weaker at night than during the day. In some locations the observed winds were nearly calm, which, together with the low temperatures between 1° and 4°C in the center of the valley, indicate the formation of a cold-air pool. The differences in the surface winds between simulations S45 and T45 were much larger at night than during the day. While both simulations produced downvalley winds, simulation T45 produced downslope and downcanyon flows that were 2–3 times stronger than those from simulation S45 so that the wind directions were in better agreement with the observations along the lower slopes of the Wasatch Mountains. Significant differences in the wind directions between the two simulations also occurred over the lower slopes of the Oquirrh Mountains. The wind speeds from both simulations were too large over the center of the valley where the observed winds were nearly calm. The surface temperatures from simulation S45 were similar to or a few degrees warmer than observed, but there was almost no spatial variation over the valley floor. The temperatures from simulation T45 were 2°C colder in the center of the valley and closer to the observed values, but the predicted temperatures in the northern end of the valley were 2°–4°C too low. The lower temperatures produced by simulation T45 are probably due to increased cold-air advection from the stronger downslope and canyon flows.

Time series of the observed and simulated wind speed, direction, and temperature are shown for sites P4 and P11 (Fig. 1) in Fig. 5 to further illustrate the dependence of model performance on location in the valley. At site P11 (Fig. 5a) near the valley center, the predicted wind speeds and directions from both simulations were similar and the wind directions agreed with the observations. The model captured the shift to upvalley flow with higher wind speeds during the first afternoon, but on the second day the shift to northerly winds occurred 2 h after the observations. The predicted wind speeds were also somewhat higher than observed at times, especially around sunrise on the second simu-

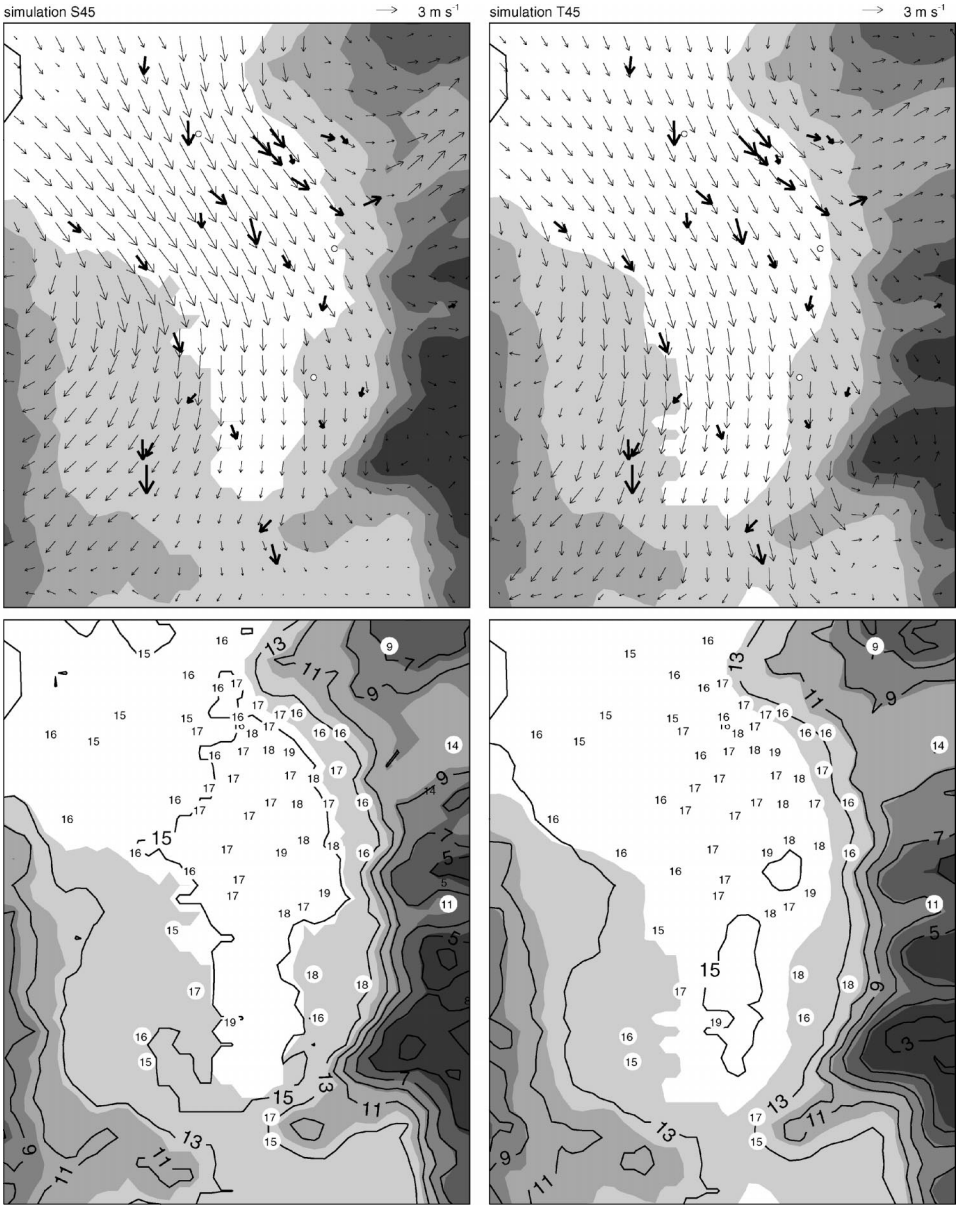


FIG. 3. Observed and simulated (top) winds and (bottom) temperatures in the Salt Lake valley at 2300 UTC (1600 MST) 16 Oct during IOP 6. Results from simulations S45 and T45 are on the left and right, respectively. Thick arrows denote observed winds, open circles denote observed wind speeds $<1$ m s$^{-1}$, thin arrows denote simulated 10 m AGL winds, small numbers denote observed temperatures in °C, and contours denote simulated 2-m temperatures. Model topography represented by gray shading with intervals at 1300, 1600, 1900, 2200, and 2500 m.

lation day. The daytime temperatures from the two simulations were nearly identical and lower than observed by 2°–3°C. The nighttime minimum temperatures from simulation S45 that were 1°–3°C too low early in the evening became nearly the same as the data a few hours before sunrise, but the temperatures from simulation T45 were 6°C too low the entire evening.

At site P4 (Fig. 5b), located about 3 km west of the base of Parleys Canyon and about 100 m higher than site P11, the magnitude of the predicted cold bias was lower than at site P11. Larger differences between the two simulations in the predicted wind speed and direction were produced at site P4 than at site P11. While the wind speeds from simulation S45 were close to the observations, the nighttime wind directions were southeasterly when the observed winds were easterly. Conversely, simulation T45 produced the observed easterly wind directions at night but the wind speeds were too high. Wind speeds around 6 m s$^{-1}$ were observed at the base of Parleys Canyon, but not at sites such as P4 a

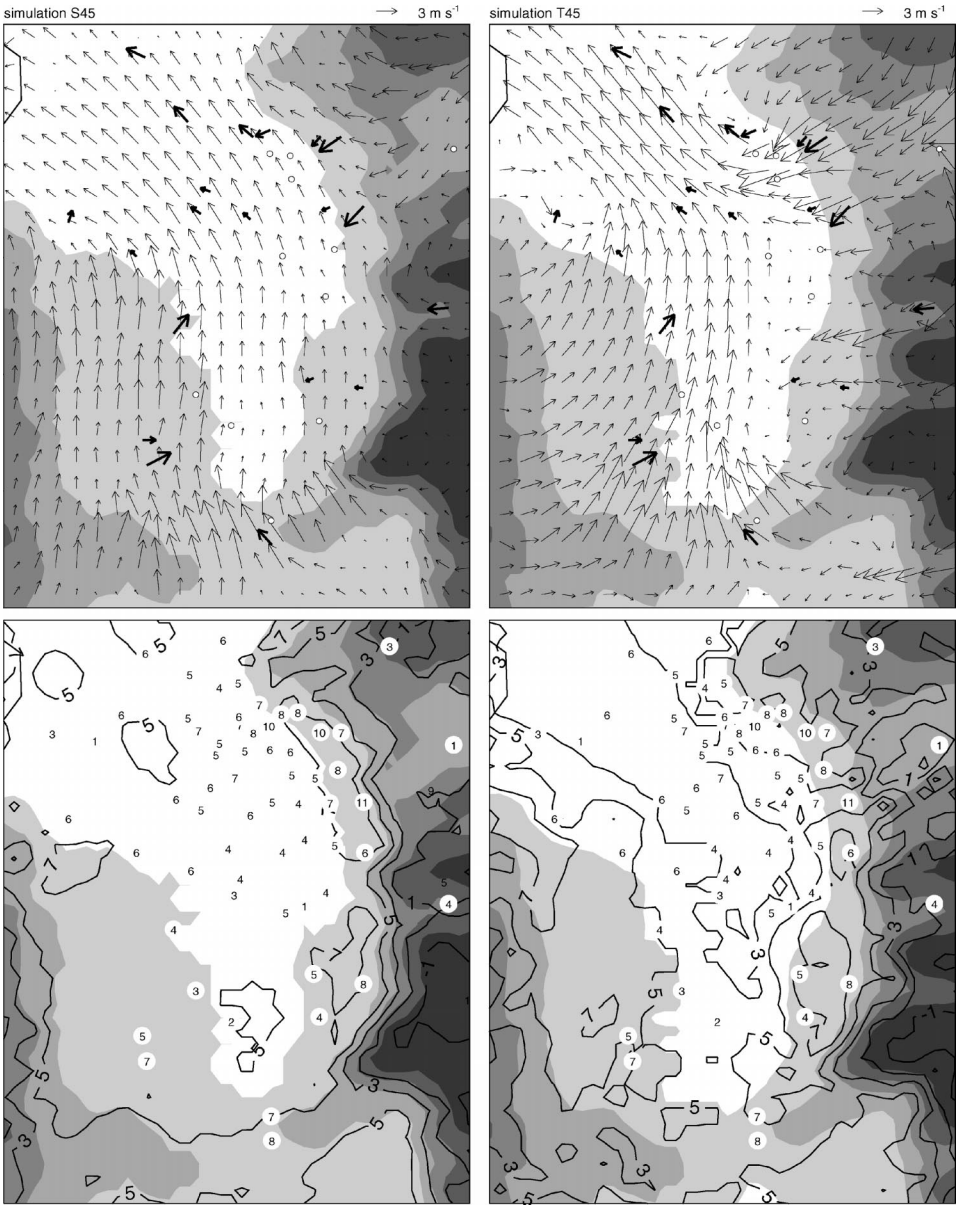


FIG. 4. Same as in Fig. 3 except at 0900 UTC (0200 MST) 17 Oct during IOP 6.

few kilometers downwind of the canyon. The observations indicated that at the surface the northeasterly flow exiting Parleys Canyon decelerates as the wind directions become easterly and then southeasterly a few kilometers west of the canyon. Neither simulation was able to capture all the characteristics of the convergence of the canyon and downvalley flows.

To determine the differences in the step-mountain and terrain-following coordinate simulations aloft, predicted wind profiles are compared to those obtained by the radar wind profiler at the Idaho National Engineering Laboratory (INEL) site (Fig. 1) in Fig. 6. Both simulations predicted the depth and strength of the northerly upvalley flows during the afternoon of 16 October, but the wind directions were northwesterly instead of northerly and the wind speeds were 1–2 m $s^{-1}$ lower than observed between 0.2 and 0.6 km AGL. While the simulated wind directions were similar to the observations during the afternoon of 17 October, the wind speeds between the surface and 0.6 km AGL were much lower than observed. During the afternoon and evening of 16 October, the predicted wind speeds above the convective boundary layer were also too low. The underprediction of the wind speeds around 2 km AGL at this time may be associated with the synoptic wind speeds from the 32-km Eta analyses that were too weak. At night, the predicted wind directions from both simulations were similar; however, the southeasterly winds between 0.2

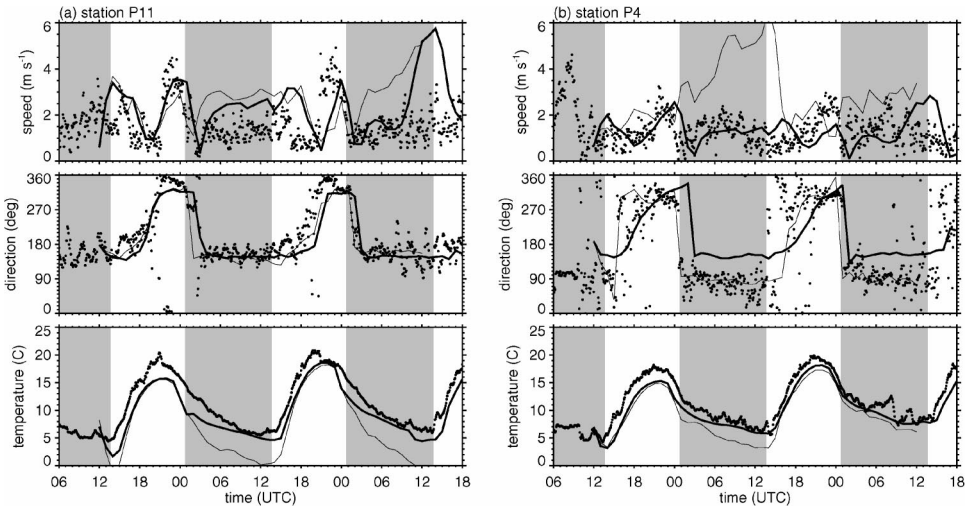


FIG. 5. Observed and simulated wind speed, direction, and temperature at sites (a) P11 and (b) P4, where dots are observations at 5-min intervals, thick line is simulation S45, and thin line is simulation T45. Gray shading indicates nighttime periods.

and 1.2 km AGL were somewhat stronger at times in simulation S45 than in simulation T45. Since both simulations employed the same boundary conditions, they both predicted increases in wind speeds above 1 km AGL during the afternoon and evening of 17 October that were associated with an approaching trough. While the nighttime wind profiles were similar to the radar wind profiler measurements during IOP 7, the wind speeds between 0.2 and 0.5 km AGL were too low and the surface wind speeds were too high several hours before sunrise as shown in Fig. 5a. The predicted wind speeds were too high at this time because the model was not able to simulate the vertical temperature gradients associated with the development of a very stable layer near the ground (not shown); therefore, the predicted winds were probably not fully decoupled from

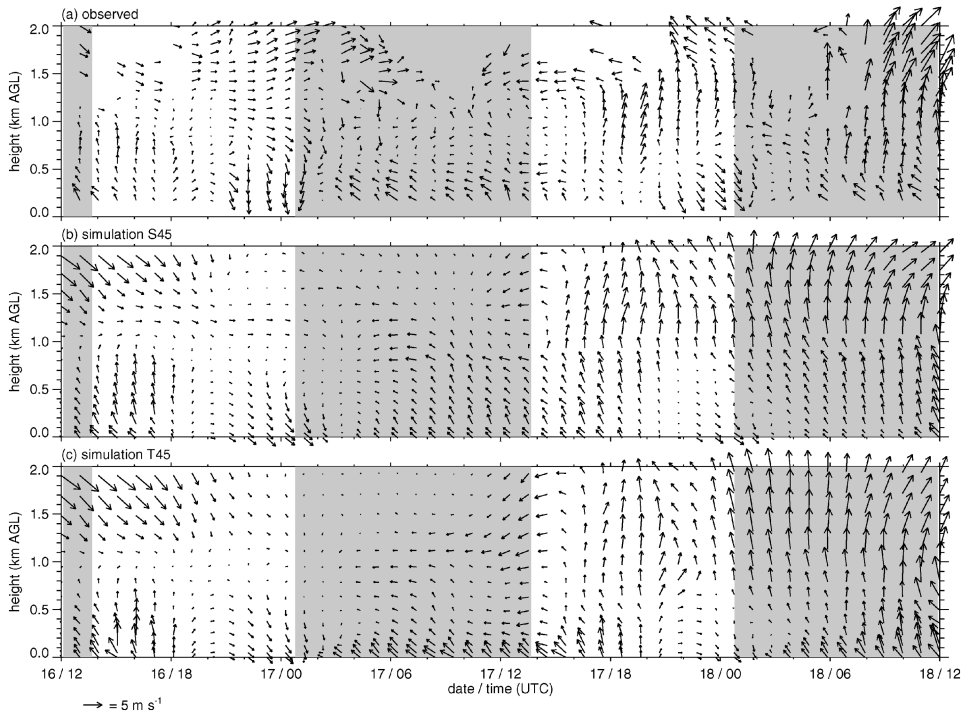


FIG. 6. (a) Observed and (b),(c) simulated wind profiles at the INEL site during IOPs 6 and 7. Gray shading denotes nighttime periods.

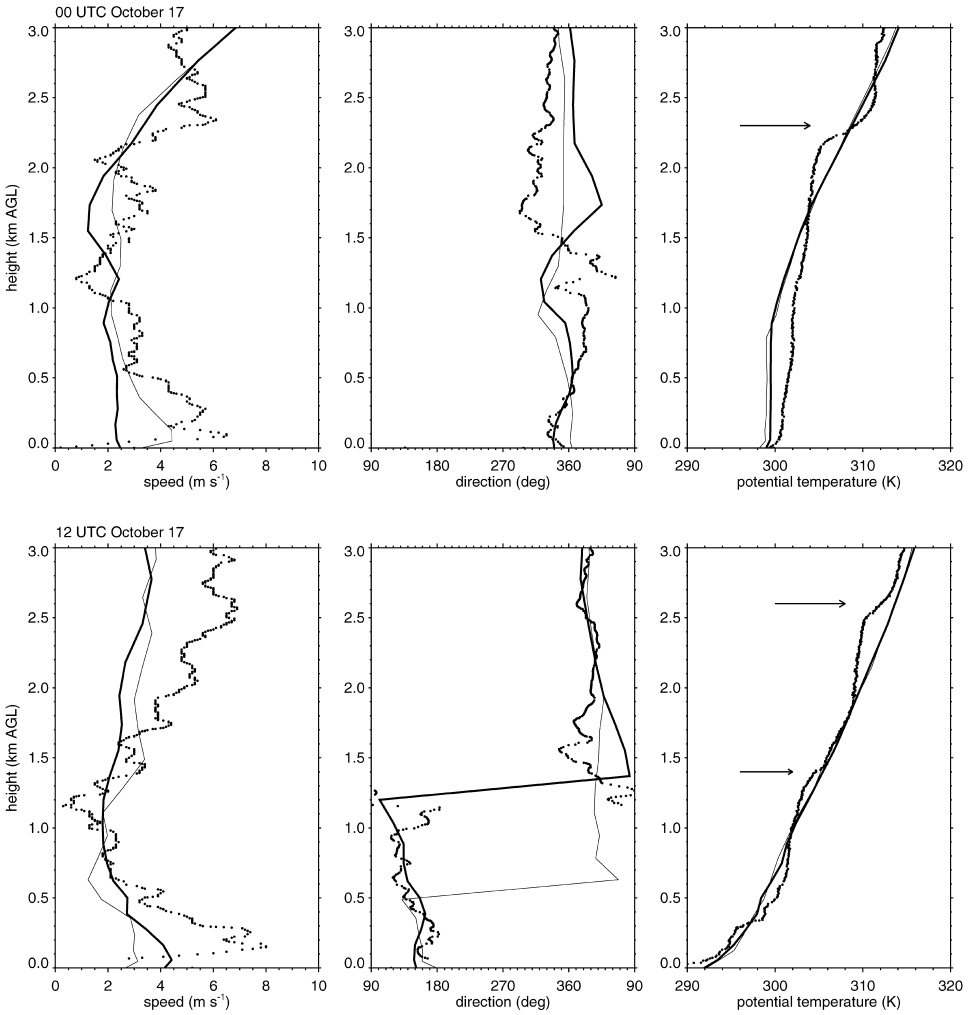


FIG. 7. Observed and simulated profiles of wind speed, direction, and potential temperature at the NCAR site at (top) 0000 and (bottom) 1200 UTC 17 Oct, where dots are observations at 5-min intervals, thick line is simulation S45, and thin line is simulation T45. Arrows denote capping inversions.

the air aloft. Figure 6 indicates that differences in the wind are not confined to the surface, but are also produced throughout the valley atmosphere at night.

The gap in the Traverse Range at the southern end of the valley is an important topographic feature that dynamically affects the flow into and out of the Salt Lake valley. As seen in the surface-simulated wind fields in Fig. 4, the southerly flow from the Provo valley accelerated over the Traverse Range and decelerated as it entered the Salt Lake valley. Observations made at the National Center for Atmospheric Research (NCAR) site (Fig. 1) often showed strong near-surface jets when the upvalley and downvalley flows were fully developed. An example of the wind profiles at the NCAR site during IOP 6 is shown in Fig. 7. During the late afternoon at 0000 UTC, a near-surface wind speed maximum of 6 m $s^{-1}$ was observed. Both models produced northerly winds, but simulation S45 did not produce a low-level wind speed maximum at this time and the wind speed maximum produced by simulation T45 was 1–2 m $s^{-1}$ too low. As drainage winds converged into the Provo valley at night and subsequently flowed into the Salt Lake valley, a southerly wind speed maximum around 8 m $s^{-1}$ was observed at 200 m AGL just before sunrise at 1200 UTC. At this time, both models produced a low-level wind speed maximum with simulation S45 somewhat closer to the observed maximum speed. Both simulated jets were too broad, however, and the wind speeds aloft above 1.5 km were too low.

The predicted potential temperature profiles from the two simulations were nearly identical and were usually within 2°C of the observed profile. The vertical grid spacing aloft was too large to resolve the observed sharp vertical temperature gradients associated with the multiple capping inversions (Fig. 7); however, both simulations may underestimate subsidence aloft as well. These capping inversions may result from secondary circulations associated with the upvalley flow that pro-

duce sinking motions over the valley center. The results from simulation S60, which had twice the number of vertical layers within the valley atmosphere, were very similar to simulation S45 at the NCAR site and at most other sites in the valley (not shown). The finer vertical grid spacing should have been sufficient to resolve some of the stable conditions in the lower valley atmosphere; however, the lack of significant improvement suggests that the forecast errors were associated with physical parameterizations, such as turbulence, rather than vertical resolution.

The behavior of the predicted thermally driven upvalley and downvalley flows over the Traverse Range is similar to the weak leeside winds produced by the Eta Model when simulating downslope windstorms (Gallus and Klemp 2000; Gallus 2000). The terrain-following simulation produced stronger acceleration over the ridge crest and higher wind speeds over the south slopes during the day (Fig. 3) and north slopes at night (Fig. 4) than the step-mountain simulation. Although the forcing mechanism of the thermally driven circulations are different than downslope windstorms, the same feature related to the vertical coordinate over the lee slopes was produced by the model.

### *b. IOP 10: Modulated terrain-induced circulations*

The strongest ambient winds among the VTMX IOPs occurred on 25 and 26 October during IOP 10. Southerly winds around 10 m $s^{-1}$ at the elevation of the surrounding mountain peaks modulated the development of the terrain-induced flows so that, in contrast to IOPs 6 and 7, diurnal low-level wind reversals did not occur. The afternoon and morning wind fields for simulations S45 and T45 are shown in Fig. 8.

During the afternoon at 2300 UTC 25 October southerly near-surface winds were observed at most of the stations in the valley. The ambient winds did not totally suppress the development of upslope flows produced by heating of the surrounding terrain. Upslope wind components are evident in the southeasterly winds over the lower slopes of the Oquirrh Mountains and the southwesterly winds over the lower slopes of the Wasatch Mountains. At this time, the results from simulation T45 are in better agreement with the observations than simulation S45. In simulation T45, the 5 m $s^{-1}$ winds over the southern valley slow to 1–2 m $s^{-1}$ over the northern valley. Simulation S45 produced wind speeds between 5 and 7 m $s^{-1}$ over most of the valley, indicating too much downward transfer of momentum to the surface.

As with the simulation for IOPs 6 and 7, the nighttime wind fields from simulations S45 and T45 were qualitatively similar with the exception that simulation T45 produced stronger flows exiting the canyons along the Wasatch Mountains. In the vicinity of Parleys Canyon, the wind speeds and directions from simulation T45 were closer to the observations. The winds predicted by simulation S45, however, were in better agreement with the observed easterly winds around 5 m $s^{-1}$ exiting Big and Little Cottonwood Canyons. In contrast with IOPs 6 and 7, the leeside winds along the Traverse Range produced by simulation T45 were stronger than simulation S45 only at night.

Radar wind profiler measurements at the INEL site indicated southerly winds from the surface up to 2 km AGL throughout the 36-h period (not shown). The predicted wind directions from simulations S45 and T45 were very similar at most elevations; however, differences in wind speed were produced in the middle of the valley atmosphere. The wind speeds and directions at the radar wind profiler range gate and the model grid layer closest to 1 km AGL are shown in Fig. 9. The predicted wind directions were nearly identical to the observations and the wind speed variations from simulation T45 prior to sunrise closely followed the observations with a decrease in wind speed during the afternoon and a gradual increase at night. The wind speeds from simulation S45 were too high during the afternoon and too low at night. Both simulations produced wind speeds that were too large after sunrise on 26 October. As with IOPs 6 and 7, the winds and temperatures from simulations S45 and S60 were nearly the same (not shown).

The stronger thermally driven circulations produced by the terrain-following coordinate may be one reason for the differences in the wind speeds over the center of the valley. Daytime upslope wind speeds that were higher in simulation T45 than in simulation S45 produced divergence in the valley atmosphere that lead to a net decrease in the southerly winds within the valley. Conversely, the higher downslope, canyon, and gap wind speeds in simulation T45 produced additional convergence in the valley at night that increased the southerly downvalley flow.

### *c. Surface statistical evaluation*

The characteristics of the valley circulations predicted by the Meso-Eta Model for other IOPs were qualitatively consistent with the results shown previously. The T45 simulations always produced stronger nighttime downslope and canyon flows and colder surface temperatures in the center of the valley than the S45 simulations. To quantify the forecast errors for the 60-h simulation of IOPs 6 and 7 and the 36-h simulations of IOPs 5, 8, and 10, the following statistical measures were employed:

bias:
$$\overline{\phi'} = \frac{1}{N}\sum_{i=1}^{N} \phi'_i; \quad \text{and} \tag{1}$$

root-mean-square error:
$$\text{rmse} = \left[\frac{1}{N-1}\sum_{i=1}^{N} (\phi'_i)^2\right]^{1/2}, \tag{2}$$

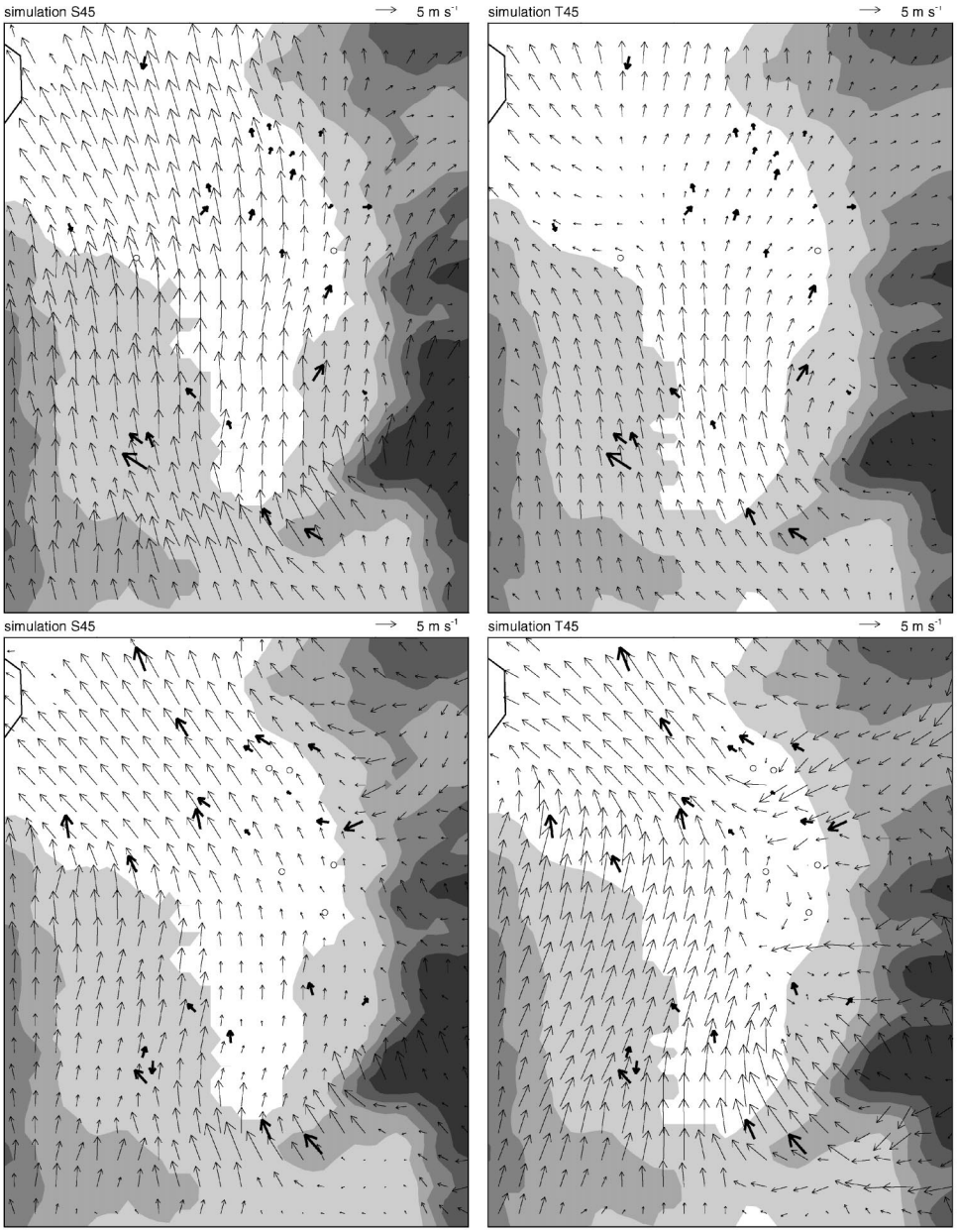


FIG. 8. Observed and simulated winds in the Salt Lake valley at (top) 2300 UTC (1600 MST) 25 Oct and (bottom) 0900 UTC (0200 MST) 26 Oct at during IOP 10. Results from simulations S45 and T45 are on the left and right, respectively. Thick arrows denote observed winds, open circles denote observed wind speeds $<1$ m s$^{-1}$, and thin arrows denote simulated 10 m AGL winds. Model topography represented by gray shading with intervals at 1300, 1600, 1900, 2200, and 2500 m.

where $\phi'$ is the difference between the hourly simulated and observed variables (simulated $-$ observed) and $N$ is 36 stations that measure both winds and temperature. Four of these stations are located just outside of the region shown in Figs. 3, 4, and 8.

The bias and rmse over daytime and nighttime periods, as well as the entire simulation period, are summarized in Table 2. The temperature biases were all negative, except for the nighttime bias from simulation S45 during IOP 5, and the biases and rmses from the S45 simulations were always smaller than those from the T45 simulations. The biases during the entire day from the S45 simulations were between $-2.34°$ and $-0.92$°C while the biases from the T45 simulations were between $-3.01°$ and $-1.47$°C. During IOPs 5, 6, 7, and 8, the nighttime cold biases and rmses were smaller than

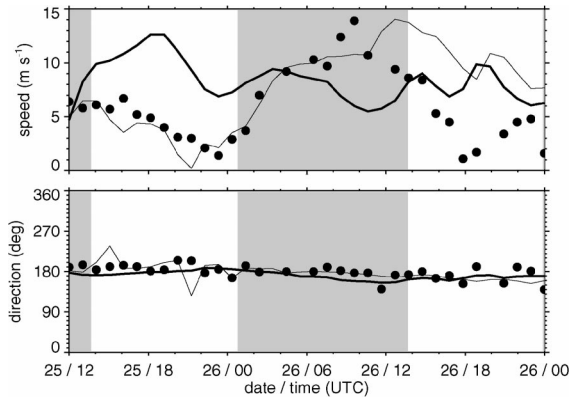


FIG. 9. Observed and simulated (top) wind speed and (bottom) direction at the INEL site at about 1 km AGL during IOP 10, where dots are hourly average observations, thick line is simulation S45, and thin line is simulation T45. Gray shading indicates nighttime periods.

the daytime values; however, the opposite situation occurred during IOP 10 when the temperature errors were significantly larger at night than during the day.

The magnitude of the average wind speed biases from simulations S45 during IOPs 5, 6, 7, and 8 were very small ($<0.2$ m s$^{-1}$). Wind speed biases from simulations T45 were greater than those from simulations S45 except during IOP 10 and the rmses from simulations T45 were usually similar to or greater than those from simulations S45. The magnitudes of the wind speed biases were greater during IOP 10 because of the higher wind speeds. For this case, the largest daytime bias was from simulation S45 and the largest nighttime bias was from simulation T45 so that the wind speed biases during the entire day for the two coordinate systems were nearly identical.

The behavior of the wind direction errors among the IOPs was more complicated. Daytime and nighttime wind direction biases for simulations T45 during IOPs 6, 7, and 8 were lower than simulations S45. A similar behavior was produced during the nighttime period of

TABLE 2. Bias (simulated − observed) and rmse [Eqs. (1) and (2)] for $N = 36$ surface stations for the VTMX IOPs simulation periods of S45 and T45.

| | IOP5 | | IOPs 6 and 7 | | IOP 8 | | IOP 10 | |
|---|---|---|---|---|---|---|---|---|
| Statistic | S45 | T45 | S45 | T45 | S45 | T45 | S45 | T45 |
| Temp (°C) | | | | | | | | |
| Daytime | | | | | | | | |
| Mean bias | −1.65 | −2.11 | −2.33 | −2.97 | −2.76 | −3.05 | −1.54 | −2.02 |
| Rmse | 2.53 | 2.94 | 2.77 | 3.40 | 3.52 | 3.98 | 2.35 | 2.97 |
| Nighttime | | | | | | | | |
| Mean bias | 0.16 | −0.51 | −1.21 | −2.42 | −1.71 | −1.75 | −3.03 | −4.51 |
| Rmse | 1.92 | 2.25 | 2.36 | 3.38 | 3.03 | 3.41 | 3.75 | 5.32 |
| All | | | | | | | | |
| Mean bias | −0.92 | −1.47 | −1.77 | −2.70 | −2.34 | −2.52 | −2.14 | −3.01 |
| Rmse | 2.31 | 2.69 | 2.57 | 3.39 | 3.33 | 3.76 | 2.99 | 4.08 |
| Wind speed (m s$^{-1}$) | | | | | | | | |
| Daytime | | | | | | | | |
| Mean bias | 0.18 | 0.44 | 0.18 | 0.56 | −0.11 | 0.24 | 1.85 | 1.29 |
| Rmse | 1.56 | 1.58 | 1.38 | 1.63 | 2.58 | 2.46 | 2.82 | 2.45 |
| Nighttime | | | | | | | | |
| Mean bias | −0.38 | 1.20 | 0.08 | 1.35 | 0.08 | 1.15 | 1.31 | 2.23 |
| Rmse | 1.44 | 2.14 | 1.45 | 2.10 | 1.81 | 2.30 | 2.12 | 2.86 |
| All | | | | | | | | |
| Mean bias | −0.04 | 0.74 | 0.13 | 0.95 | −0.03 | 0.60 | 1.64 | 1.67 |
| Rmse | 1.51 | 1.82 | 1.41 | 1.88 | 2.31 | 2.40 | 2.56 | 2.62 |
| Wind direction (°) | | | | | | | | |
| Daytime | | | | | | | | |
| Mean bias | −2.86 | −10.23 | −9.88 | 5.04 | −2.81 | 0.83 | −3.58 | −5.33 |
| Rmse | 77.69 | 90.91 | 66.96 | 59.86 | 80.89 | 84.53 | 61.37 | 57.64 |
| Nighttime | | | | | | | | |
| Mean bias | −12.33 | −8.98 | 11.73 | 3.23 | 7.57 | −5.83 | 15.28 | 4.94 |
| Rmse | 87.69 | 89.86 | 70.01 | 55.49 | 80.49 | 87.33 | 60.47 | 52.32 |
| All | | | | | | | | |
| Mean bias | −6.59 | −9.74 | 0.85 | 4.14 | 1.30 | −1.81 | 3.89 | −1.27 |
| Rmse | 81.78 | 90.50 | 68.49 | 57.73 | 80.73 | 85.65 | 61.02 | 55.60 |

TABLE 3. Summary of performance of the step-mountain and terrain-following vertical coordinates for specific atmospheric quantities in the Salt Lake valley during the VTMX IOPs. An ex (X) denotes which simulation performed better in general and an ex in both columns indicates that there was not a significant difference between the simulations.

| Parameter | Vertical coordinate | |
|---|---|---|
| | Step mountain | Terrain following |
| Surface temperatures | X | |
| Surface wind speeds | X | |
| Surface wind directions (valley center) | X | X |
| Surface wind directions (valley sidewalls) | | X |
| Parleys Canyon wind speed | X | |
| Parleys Canyon wind direction | X | X |
| Daytime flow through Traverse Gap | | X |
| Nighttime flow through Traverse Gap | X | |
| Valley wind speeds above the surface | | X |
| Time of shift from downvalley to upvalley flow | X | |
| Boundary layer depth | X | X |

IOPs 5 and 10, but the wind direction errors from simulations T45 were larger than simulations S45 during the daytime period.

The statistics in Table 1 suggests that the relative performance of the step-mountain and terrain-following coordinate depends upon the synoptic forcing. As discussed in Doran et al. (2002), IOPs 5, 6, and 8 were characterized by well-developed thermally driven circulations and weak winds aloft at crest level. Similar conditions were observed during IOP 7, except that the increase in upper-level wind speeds began to affect the near-surface flows a few hours before sunrise. Valley circulations were influenced by ambient winds throughout IOP 10. Consistent with the IOP classifications, the biases and rmses in temperature, wind speed, and direction from IOPs 5, 6, 7, and 8 were usually similar to each other and different from those produced for IOP 10.

A subjective assessment of the model performance for specific parameters is summarized in Table 3 based on the statistics and other qualitative comparisons of model output with observations. As indicated by Table 3 and the previous results, the step-mountain and terrain-following coordinate simulations each have their own advantages and disadvantages when simulating circulations in the Salt Lake valley.

### *d. Operational considerations*

The Meso-Eta Model was able to qualitatively simulate most of the dominant circulations observed in the Salt Lake valley during VTMX, including the diurnal reversal of valley, slope, and canyon flows. At certain locations one would not expect the forecasts to be perfectly accurate. For example, the 850-m horizontal grid spacing still does not represent the terrain variations in the Traverse Range gap (the NCAR site) and around meteorological stations on steep slopes or in the middle of canyons located along the Wasatch Mountains. Nevertheless, the forecasts produced by the operational 32-km NCEP Eta Model are not able to predict the spatial variations in the valley circulations obtained in this study. While the 10-km Eta Model would have a number of points inside the valley, it is unlikely that it could resolve the interactions of the valley, slope, and canyon flows. The 10-km grid spacing also poorly resolves the slope of the Wasatch Front, which may be one reason for the underestimation of the downslope windstorm strength as described by Staudenmaier and Mittelstadt (1997).

Another feature the model cannot simulate is the urban heat island effect. Observed nighttime temperatures over a portion of downtown Salt Lake City were usually a few degrees warmer than other stations at similar elevations in the valley (Fig. 4). Since the model is used at larger spatial scales, there has not been a need to incorporate an urban canopy parameterization.

The performance of the Meso-Eta Model in simulating the boundary layer properties and valley circulations was similar to other mesoscale models. In a companion paper, Zhong and Fast (2003) compared the results of MM5, RAMS, and Meso-Eta (using the step-mountain vertical coordinate) for IOPs 6, 7, and 10. MM5 and RAMS also produced a cold bias in the surface temperatures. The step-mountain and terrain-following coordinate simulations in this study also produced cold biases (Table 2), although somewhat different temperatures were predicted over the valley floor at night (Fig. 4). This suggests that the temperature errors were associated with errors in the surface layer, turbulence, soil, and vegetation parameterizations in the models, rather than the vertical coordinate. Apparently because of the similar vertical coordinates, the predicted wind directions from RAMS and MM5 were closer to those produced by the terrain-following coordinate in the Meso-Eta Model than those produced by the step-mountain coordinate.

Computational requirements and numerical stability are important considerations for operational forecasting. In this study, the time steps employed by the step-mountain coordinate simulations varied between 1 and 2 s; however, the time steps used by the terrain-following

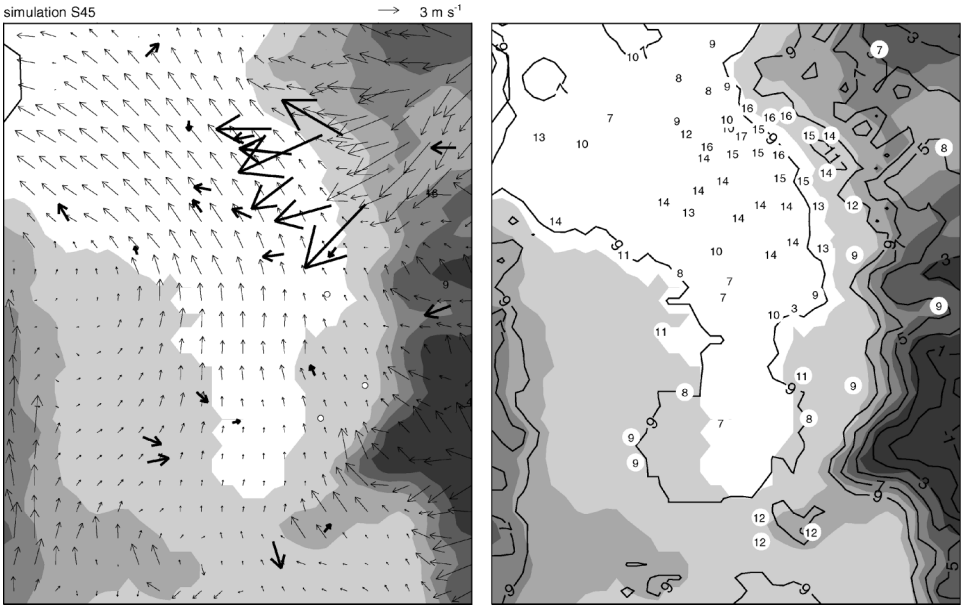


FIG. 10. Observed and simulated (left) winds and (right) temperatures in the Salt Lake valley at 0600 UTC (2300 MST) 8 Oct during IOP 3. Thick arrows denote observed winds, open circles denote observed wind speeds $<1$ m s$^{-1}$, thin arrows denote simulated 10 m AGL winds, numbers denote observed temperatures in °C, and contours denote simulated 2-m temperatures. Model topography represented by gray shading with intervals at 1300, 1600, 1900, 2200, and 2500 m.

coordinate system were much smaller, between 0.1 and 1 s. The computational time required by the terrain-following coordinate was as much as 10 times more than for the step-mountain coordinate for the same simulation period. A smaller time step was required because the larger wind speeds along the valley sidewalls in the terrain-following simulations also produced larger vertical motions so that the Courant–Friedrichs–Lewy (CFL) condition was violated. A remaining problem that requires attention is that the terrain-following coordinate simulations often became numerically unstable when the near-surface flows were particularly strong.

For example, the terrain-following coordinate simulations became numerically unstable during strong downslope windstorm events. Downslope windstorms, such as those along the Front Range of Colorado (e.g., Lilly et al. 1982), are produced by mountain waves and wave breaking aloft (Durran 1990). In addition to lower-tropospheric synoptic pressure gradients that produce easterly winds around the 700-hPa level, downslope windstorms in Salt Lake City are also associated with the presence of a cold air mass located over the Wyoming (Holland 2002). Strong flows are channeled through Parleys Canyon, the lowest gap in the Wasatch Mountains, during these events. Air temperatures increase as a result of adiabatic warming as the flow descends into the Salt Lake valley. Prior to the VTMX campaign, no observations above the surface were available to examine the characteristics of downslope windstorms in Salt Lake City. Particularly strong downslope flows over the northeastern end of the valley occurred on two of the IOPs.

To examine the performance of the Meso-Eta Model for these conditions, a 36-h simulation was performed using the step-mountain coordinate for IOP 3. As shown in Fig. 10, during the evening at 0600 UTC (2300 MST) on 8 October winds in excess of 10 m s$^{-1}$ were observed at several stations west of Parleys Canyon. Adiabatic warming and subsequent mechanical vertical mixing within the high wind regions produced surface temperatures between 14° and 17°C, which were 10°C higher than other locations along the valley floor. Predicted wind speeds over Parleys Canyon were greater than 10 m s$^{-1}$; however, weak southeasterly winds between 2 and 3 m s$^{-1}$ were produced over the northeastern end of the valley where strong winds were observed. Because the Meso-Eta Model did not produce strong winds in this region, the temperatures were too low as well.

Radar wind profiler observations at the INEL site during IOP 3 in Fig. 11 show that the easterly winds exiting Parleys Canyon propagated over the convective boundary layer between 0.5 and 1 km AGL throughout the afternoon of 7 October. After the collapse of the convective boundary layer, the thermally driven upslope flows that opposed the easterly flow diminished so that strong winds were produced at the surface as well. While simulation S45 qualitatively produced strong easterly flow found 1 km AGL over the convective boundary layer, the upvalley flows of 5 m s$^{-1}$ were stronger than the 2 m s$^{-1}$ observed wind speeds. At

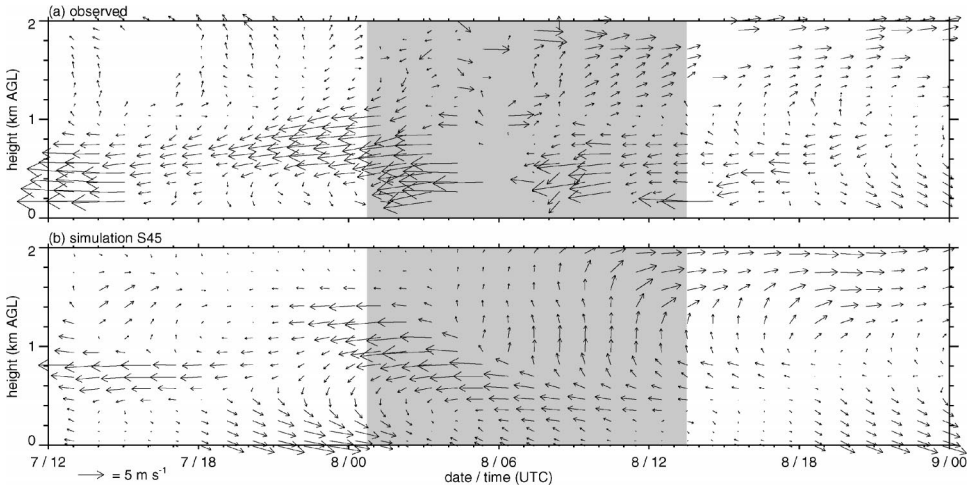


FIG. 11. (a) Observed and (b) simulated S45 wind profiles at the INEL site during IOP 3. Gray shading denotes nighttime periods.

night, the simulated winds aloft were similar to the profiler measurements; however, the winds did not propagate to the ground. This suggests that vertical momentum transfer was not properly represented during the nighttime stable conditions. These results are also consistent with the coarser horizontal resolution simulations of Gallus (2000), Gallus and Klemp (2000), and Staudenmaier and Mittelstadt (1997) in which the leeside wind speeds were underpredicted during downslope windstorm events.

## 5. Summary

An evaluation of the performance of the Meso-Eta Model in simulating valley circulations with grid spacing smaller than 1 km has been presented. The Meso-Eta Model was able to qualitatively forecast the diurnal evolution of the dominant circulations in the Salt Lake valley including valley, slope, and canyon flows and their modification by synoptic forcing during five IOPs. The evaluation of the Meso-Eta Model using the VTMX field campaign observations indicated that the step-mountain and terrain-following vertical coordinates each has its own advantages and disadvantages when simulating the evolution of boundary layer properties and valley circulations within the Salt Lake valley. Neither vertical coordinate outperformed the other overall.

In general, the nighttime near-surface temperatures and wind speeds from the step-mountain coordinate simulations were closer to the observations at most locations, while the terrain-following coordinate simulations reproduced the observed surface wind directions over the valley sidewalls better. The largest differences in the simulated surface wind direction occurred at night. The terrain-following coordinate system better represented the observed nocturnal convergence of downslope and canyon flows into the valley, but the wind speeds over the steeper slopes were too high. The high wind speeds lead to too much cold-air advection so that the surface temperatures were often 5°C lower than observed over the valley center. The near-surface daytime and nighttime cold bias produced by both vertical coordinates in the Meso-Eta Model was also produced by similar MM5 and RAMS mesoscale model simulations of the Salt Lake valley (Zhong and Fast 2003). Differences in the wind speed and direction were also produced at night in the middle of the valley atmosphere several hundred meters above the ground, and the terrain-following coordinate simulation performed somewhat better than the step-mountain coordinate at these elevations. However, the differences between the step-mountain and terrain-following coordinate simulations were usually very small above the height of the surrounding mountains.

The numerical treatment of the pressure gradient term and other horizontal gradients is one factor contributing to the forecast errors because the local slopes in the Salt Lake valley are often relatively steep. The wind fields from the two sets of simulations were significantly different at night over the valley sidewalls, resulting in different vertical advection. The results also indicate that forecast errors associated with physical parameterizations, such as turbulence, were probably as important or more so than those associated with the choice of vertical coordinate. For example, errors in the near-surface winds and temperatures sometimes appear to be associated with vertical momentum transfer that is either too large or too small during stable conditions. Increasing the number of vertical levels in the valley atmosphere did not significantly improve the wind and temperature profiles.

For this high-resolution application, the step-mountain coordinate did not require as small of a time step for the CFL numerical stability criteria as the terrain-following coordinate. The terrain-following coordinate simulations were not stable for reasonable time steps

during periods of very strong winds within a few hundred meters of the ground, such as those during downslope windstorms. The step-mountain coordinate simulation was able to simulate the development of a downslope windstorm, but similar to previous studies (e.g., Staudenmaier and Mittelstadt 1997) the wind speeds did not propagate down to the surface over the center of the valley at night and during the morning. This problem, however, did not occur frequently in this study because the focus of the VTMX field campaign IOPs was on local thermally driven circulations in which the synoptic winds were usually weak at the elevation of the surrounding mountain peaks. From an operational standpoint, the advantage of the numerical stability of the step-mountain coordinate is that a wider range of atmospheric conditions can be simulated within basins and valleys using a subkilometer grid spacing, but this vertical coordinate will result in certain systematic forecast errors.

*Acknowledgments.* I would like to thank Matthew Pyle of NCEP for his assistance with the Meso-Eta Model and Shiyuan Zhong, Chris Doran, and the reviewers for their comments on this paper. This work was supported by the U.S. Department of Energy, under the auspices of the Atmospheric Sciences Program of the Office of Biological and Environmental Research. PNNL is operated for the U.S. DOE by Battelle Memorial Institute.

## REFERENCES

Angevine, W. M., and K. Mitchell, 2001: Evaluation of the NCEP mesoscale Eta Model convective boundary layer for air quality applications. *Mon. Wea. Rev.,* **129,** 2761–2775.

Black, T. L., 1994: The new NMC mesoscale Eta Model: Description and forecast examples. *Wea. Forecasting,* **9,** 265–278.

Carroll, J. J., L. R. Mendez-Nunez, and S. Tanrikulu, 1987: Accurate pressure gradient calculations hydrostatic atmospheric models. *Bound.-Layer Meteor.,* **41,** 149–169.

Danard, M., Q. Zhang, and J. Kozloski, 1993: On computing the horizontal pressure gradient force in sigma coordinates. *Mon. Wea. Rev.,* **121,** 3173–3183.

Doran, J. C., J. D. Fast, and J. Horel, 2002: The VTMX 2000 campaign. *Bull. Amer. Meteor. Soc.,* **83,** 537–551.

Dudhia, J., 1993: A nonhydrostatic version of the Penn State–NCAR Mesoscale Model: Validation tests and simulation of an Atlantic cyclone and cold front. *Mon. Wea. Rev.,* **121,** 1493–1513.

Durran, D. R., 1990: Mountain waves and downslope winds. *Atmospheric Processes over Complex Terrain, Meteor. Monogr.,* No. 45, Amer. Meteor. Soc., 59–81.

Gallus, W. A., 2000: The impact of step orography on flow in the Eta Model: Two contrasting examples. *Wea. Forecasting,* **15,** 630–637.

——, and J. B. Klemp, 2000: Behavior of flows over step orography. *Mon. Wea. Rev.,* **128,** 1153–1164.

Holland, L., 2002: Downslope windstorms along the Wasatch Front. M.S. thesis, Dept. of Meteorology, University of Utah, Salt Lake City, UT, 86 pp.

Janjić, Z. I., 1994: The step-mountain coordinate model: Further developments of the convective viscous sublayer, and turbulence closure schemes. *Mon. Wea. Rev.,* **122,** 927–945.

——, J. P. Gerrity Jr., and S. Nickovic, 2001: An alternative approach to nonhydrostatic modeling. *Mon. Wea. Rev.,* **129,** 1164–1178.

Lilly, D. K., J. M. Nichols, R. M. Chervin, P. J. Kennedy, and J. B. Klemp, 1982: Aircraft measurements of wave momentum flux over the Colorado Rocky Mountains. *Quart. J. Roy. Meteor. Soc.,* **108,** 625–642.

Mahrer, Y., 1984: An improved numerical approximation of the horizontal gradients in a terrain-following coordinate system. *Mon. Wea. Rev.,* **112,** 918–922.

Manobianco, J., and P. A. Nutter, 1999: Evaluation of the 29-km Eta Model: Part II: Subjective verification over Florida. *Wea. Forecasting,* **14,** 18–37.

Mesinger, F., 1996: Improvements in quantiative precipitation forecasts with the Eta regional model at the National Centers for Environmental Prediction: The 48-km upgrade. *Bull. Amer. Meteor. Soc.,* **77,** 2637–2649.

——, and T. L. Black, 1992: On the impact of forecast accuracy of the step-mountain (Eta) vs. sigma coordinate. *Meteor. Atmos. Phys.,* **50,** 47–60.

——, Z. L. Janjić, S. Nickovic., D. Gavrilov, and D. G. Deaven, 1988: The step-mountain coordinate: Model description and performance for cases of Alpine lee cyclogenesis and for a case of Appalachian redevelopment. *Mon. Wea. Rev.,* **116,** 1493–1518.

Michalakes, J., S. Chen, J. Dudhia, L. Hart, J. Klemp, J. Middlecoff, and W. Skamarock, 2001: Development of a next-generation of regional weather research and forecast model. *Developments in Teracomputing: Proceedings of the Ninth ECMWF Workshop on the Use of High Performance Computing in Meteorology,* World Scientific, 269–276.

O'Conner, W. P., D. J. Schwab, and G. A. Lang, 1999: Forecast verification for Eta Model winds using Lake Erie storm surge water levels. *Wea. Forecasting,* **14,** 119–133.

Pielke, R. A., 1984: *Mesoscale Meteorological Modeling.* Academic Press, 612 pp.

——, and Coauthors, 1992: A comprehensive meteorological modeling system—RAMS. *Meteor. Atmos. Phys.,* **49,** 69–91.

Rogers, E., T. L. Black, D. G. Deaven, G. J. DiMego, Q. Zhao, M. Baldwin, N. W. Junker, and Y. Lin, 1996: Changes to the operational ''early'' Eta analysis/forecast system at the National Centers for Environmental Prediction. *Wea. Forecasting,* **11,** 391–413.

Staudenmaier, M. J., and J. Mittelstadt, 1997: Results of the western region evaluation of the Eta-10 model. Western Region Tech. Attachment 97-18, 8 pp. [Available from National Weather Service Western Region-SSD, Rm. 1311, 125 S. State St., Salt Lake City, UT 84147.]

Xue, M., K. K. Droegemeier, and V. Wong, 2000: The Advanced Regional Prediction System (ARPS)—A multi-scale nonhydrostatic atmospheric simulation and prediction model. Part I: Model dynamics and verification. *Meteor. Atmos. Phys.,* **75,** 161–193.

Zhong, S., and J. D. Fast, 2003: An evaluation of the MM5, RAMS, and Meso-Eta at subkilometer resolution using VTMX field campaign data in the Salt Lake valley. *Mon. Wea. Rev.,* **131,** 1301–1322.